Stator-flux-oriented control of a doubly-fed induction machine with and without position encoder

B.Hopfensperger, D.J.Atkinson and R.A.Lakin

Abstract: The control of a doubly-fed induction machine (DFM) with and without the use of a rotor position encoder is examined. First, a stator flux linkage oriented control scheme for power and speed control, with a position encoder, shows the high performance control capabilities of this control arrangement and serves as foundation for the sensorless scheme. The power-control method is then applied to a sensorless method, based on a previous control arrangement. This method is then extended to derive a sensorless speed-control mechanism for the DFM. All control schemes are implemented and performed on an experimental test system, comprising two 80C167 microcontrollers and a 2.25kW wound rotor induction machine.

List of symbols

f_1, f_2 = stator and rotor frequency, electrical Hz
f_m = mechanical frequency of rotor, mechanical Hz
$\bar{i}_1, \bar{i}_2$ = stator and rotor current space vector
L_1, L_2 = stator and rotor self inductance
L_m = mutual inductance
n_m = mechanical speed of rotor, r/min
P_1, Q_1 = stator active and reactive power
p_A = machine pole-pair number
R_1, R_2 = stator and rotor resistance
T_e = electromagnetic torque
V_1 = stator phase voltage, rms
$\bar{v}_1, v_2$ = stator and rotor voltage space vector
α_1 = stator voltage vector angle within frame 'a', electrical rad
β_2 = rotor current vector angle within frame 'b', electrical rad
ε = angle between frame 'b' and 'e', electrical rad
Θ_m = rotor angle, mechanical rad
Θ_r = rotor angle, electrical rad
μ = angle between frame 'a' and 'e', electrical rad
χ = rotor current vector angle within frame 'e', electrical rad
$\bar{\Psi}_1, \bar{\Psi}_2$ = stator and rotor flux linkage space vector
ω_1, ω_2 = angular frequency of stator and rotor quantities, electrical rad/s
ω_r = mechanical angular frequency of rotor, electrical rad/s
ω_e = angular frequency of the excitation reference frame, electrical rad/s

Superscripts:

a = stator (stationary) reference frame
b = rotor reference frame
e = excitation reference frame for orientation
g = general reference frame
$*$ = indicating a demand value

IEE Proceedings online no. 20000442

DOI: 10.1049/ip-epa:20000442

Paper first received 27th October 1999 and in revised form 14th March 2000

B. Hopfensperger is with Siemens plc, Standard Drives, Varey Road, Congleton, Cheshire, CW12 1PH, UK

D.J. Atkinson is with the Department of Electrical and Electronic Engineering, University of Newcastle upon Tyne, Merz Court, Newcastle upon Tyne, NE1 7RU, UK

R.A. Lakin is with Microtech Ltd., Hawks Road Industrial Estate, Unit 13, Gateshead, NE8 3BL, UK

1 Introduction

Connecting the stator windings of a wound rotor induction machine to a stiff voltage supply and the rotor windings to a bi-directional power converter constitutes a doubly-fed machine arrangement. It is referred to as a doubly-fed induction machine (DFM) in this paper. The potential of doubly-fed machines, in general, for variable speed drive applications, with the main advantage of a reduced power converter rating, which is related to the desired speed range, is well known [1]. Applications far into the megawatt region are reported [2]. A high performance field-oriented control method for the DFM was introduced by Leonhard [3] 20 years ago. The rotor current vector is oriented into a reference frame aligned with the stator flux, enabling the torque and the stator active power to be directly manipulated with the q-component of the rotor current vector. Since the flux in the machine is mainly determined by the stiff stator voltage, this enables the stator reactive power to be controlled by the d-component of the rotor current vector. Controlling the DFM with this field-oriented method leads to stable control performance [4, 5], where the damping of the system can be positively influenced by reducing the current-control loop bandwidth [5].

This stator-flux-oriented control principle makes use of a rotor position encoder and is now well established in research and industry. Owing to the decoupled active and reactive control possibilities, the main area of application

for the DFM is in variable-speed generating systems such as wind power [6, 7] and hydro power [8].

One important goal of past and ongoing research is to avoid the use of an encoder for position and speed feedback for a drive or generator application with induction machines, especially for cage induction machines. DFM arrangements have not received as much attention in comparison. The aim of this paper is to investigate this particular area of machine control, i.e. power-control applications and also speed-control applications with a DFM.

In [9], a stator-flux-oriented sensorless active and reactive power-control scheme is introduced, which takes advantage of the proportionalities between stator and rotor quantities. Limitations of that control result for low rotor-current magnitudes, as will be shown in this paper. A different method [10] is based on air-gap flux orientation, in which the machine torque and flux are estimated by sensing the rotor current and voltage. These estimates are then used for derivation of a torque angle, which serves as a feed-back to the control scheme and which also allows sensorless speed control. It seems, however, that this arrangement requires an analogue voltage-controlled oscillator. Another sensorless DFM control contribution [11] is based on the scheme in [9]. Describing different modes of operation [11] and the engineering of a DFM drive arrangement. the sensorless speed-control method relies on the differentiation of the estimated rotor-position angle.

This paper focuses on the control issues for the DFM, for control with and without a position sensor. The first part of this paper summarises the stator-flux-oriented DFM control with a position sensor. It serves as a basis and a performance comparison for the development of the sensorless scheme. The limitation of the method in [9] is highlighted, and it is then further developed to be applicable for sensorless speed control. An alternative angle construction method in contrast to that in [9, 11] is also presented.

2 Experimental arrangements

The following control investigation of the DFM will be better understood if the experimental equipment is first described.

The complete laboratory arrangement is illustrated in Fig. 1. The power circuit (thickened lines) consists of a bi-directional power converter and the DFM. A 3.75kW DC-machine (not shown in Fig. 1) acts as a prime mover to the system in the generating mode. The independently functioning front end of the bi-directional power converter creates a unity power factor interface at its grid connection point and controls the DC-link voltage to 650 V. The gate drive circuits of the machine-side inverter module are interfaced to the PWM signals coming from the external controller unit.

The control hardware comprises two paralleled 16-bit fixed point 80C167 microcontrollers, denoted as μC1 and μC2 in Fig. 1. Microcontroller μC1 performs most of the control functions, which include current control with pulse-width modulation (PWM) generation, position and speed calculation. The microcontroller's PWM unit generated interrupt request sets at the switching frequency of the machine-side inverter and also determines the available processing time. A switching frequency of 2.5kHz was chosen, which gives 400μs for software execution. Microcontroller μC2 performs the remaining functions such as angle calculation, power calculation and power control. A high-speed serial link provides the communication link between both microcontrollers. The 10 bit A/D conversion for the measured quantities is shared between the microcontrollers depending on the respective control functions. The sensed quantities are the stator voltage, the stator current and the rotor current.

Various interface circuits allow electrical isolation between power and control hardware. Incremental encoder signals are received in a timer unit of μC1 for position and speed calculation. μC1 produces control variables for data

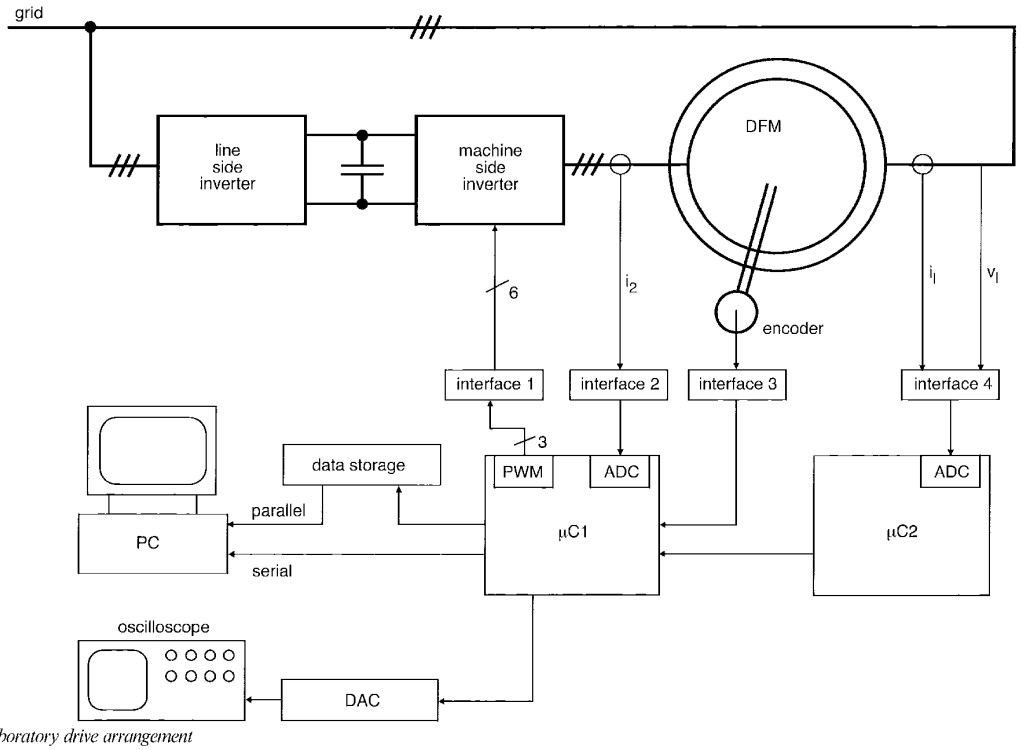

Fig. 1 *Laboratory drive arrangement*

storage and monitoring purposes on the PC and an oscilloscope.

The wound rotor induction machine employed for experimental work is a 2.25kW (3 HP) machine with 2 pole-pairs. Its synchronous speed lies at 1500r/min with a rated speed of 1420r/min. The stator is rated for 420V at 8A and the rotor for 390V at 6A.

3 Stator-flux-linkage-oriented control of the DFM

3.1 General features

The features described in this Section are common to control schemes with a sensor and without a sensor. They form the basis for both control schemes.

3.1.1 Dynamic model and reference frames: Considering the electromagnetic torque of the DFM in a general reference frame 'g' in space-vector representation

$$T_e = -\frac{3}{2}p_A\frac{L_m}{L_1}\left(\overline{\Psi}_1^g \times \bar{i}_2^g\right) = -\frac{3}{2}p_A\frac{L_m}{L_1}\left(\Psi_{d1}^g i_{q2}^g - \Psi_{q1}^g i_{d2}^g\right) \quad (1)$$

then it can be seen that for choosing a reference frame which is attached to the stator flux linkage Ψ_1, eqn. 1 would change to the following simple form

$$T_e = -\frac{3}{2}p_A\frac{L_m}{L_1}\Psi_1^e i_{q2}^e \quad (2)$$

since

$$\Psi_{q1}^e = 0 \qquad \Psi_{d1}^e = \left|\overline{\Psi}_1^g\right| = \Psi_1^e \quad (3)$$

The reference frame attached to the stator flux is denoted as the excitation 'e' reference frame. Stator quantities are marked with a subscript 1 and rotor quantities with a 2. Eqn. 2 shows that the torque of the DFM can be controlled by the q-component of the rotor current in the e-frame, when the stator flux is held at a constant value.

The dynamic machine equations presented in the excitation reference flame e are [12]

$$\overline{v}_1^e = R_1\bar{i}_1^e + \frac{d\overline{\Psi}_1^e}{dt} + \mathrm{j}\omega_e\overline{\Psi}_1^e \quad (4)$$

$$\overline{v}_2^e = R_2\bar{i}_2^e + \frac{d\overline{\Psi}_2^e}{dt} + \mathrm{j}(\omega_e - \omega_r)\overline{\Psi}_2^e \quad (5)$$

$$\overline{\Psi}_1^e = L_1\bar{i}_1^e + L_m\bar{i}_2^e \quad (6)$$

$$\overline{\Psi}_2^e = L_2\bar{i}_2^e + L_m\bar{i}_1^e \quad (7)$$

Reference frames for the DFM in the field orientation with angle and angular speed definitions are displayed in Fig. 2.

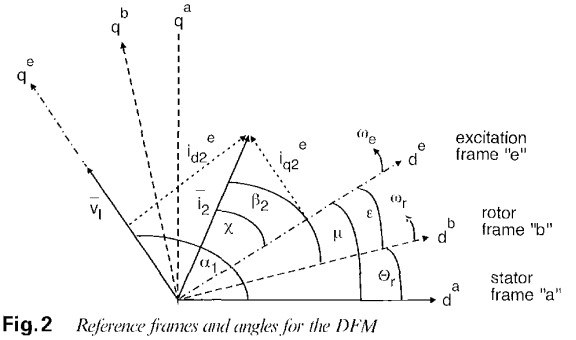

Fig. 2 *Reference frames and angles for the DFM*

3.1.2 Stator-flux angle μ determination: The stator-flux-oriented control scheme of the DFM makes it essential to determine the stator-flux vector within the stationary reference frame 'a'. There are mainly three different ways to obtain the stator-flux angle μ.

First, by looking at the stator-flux equation in the stator reference frame a:

$$\overline{\Psi}_1^a = L_1\bar{i}_1^a + L_m\bar{i}_2^a$$

and by splitting it into its d-q-components, then μ follows as

$$\mu = \arctan\frac{\Psi_{q1}^a}{\Psi_{d1}^a} \quad (8)$$

In this case it is first required to transform the rotor-current vector into the stationary stator reference frame with the help of the rotor-position angle. The individual stator-flux components can then be calculated by

$$\Psi_{d1}^a = L_1 i_{d1}^a + L_m i_{d2}^a \qquad \Psi_{q1}^a = L_1 i_{q1}^a + L_m i_{q2}^a \quad (9)$$

This way makes it essential that both currents are measured and the inductance values of the machine are known. Also, the rotor-position angle has to be known.

A second possible way of acquiring μ is by considering the stator-voltage equation in the stationary frame.

$$\overline{v}_1^a = R_1\bar{i}_1^a + \frac{d\overline{\Psi}_1^a}{dt} \quad (10)$$

The two flux components can now be calculated by integration:

$$\Psi_{d1}^a = \int\left(v_{d1}^a - R_1 i_{d1}^a\right)dt$$

$$\Psi_{q1}^a = \int\left(v_{q1}^a - R_1 i_{q1}^a\right)dt \quad (11)$$

This method may make it essential to employ a digital passband filter with a low cutoff frequency to avoid DC-offsets [6]. Here the stator current and voltage have to be sensed and the stator resistance value has to be known. However, the rotor position is not needed.

A third and commonly used method simplifies eqn. 10 by neglecting the stator resistance. This approach can be justified for larger machines, since the resistance in comparison to the stator reactance is quite small ($R_1 << \omega_1 L_1$) [12]. Eqn. 10 can in simple terms be written as

$$\overline{v}_1^a \approx \frac{d\overline{\Psi}_1^a}{dt} \quad (12)$$

From this, it can be seen that a reference frame attached to the stator flux has the same angular frequency as the stator voltage in steady-state conditions

$$\omega_e = \omega_1 = const \quad (13)$$

By substituting $\overline{\Psi}_1^a = |\overline{\Psi}_1^a|e^{j\mu}$ in eqn. 12 and applying the rules of differentiation, the magnitude of the stator flux expressed in the e-frame results as

$$\Psi_1^e \approx \frac{\sqrt{2}V_1}{\omega_1} \quad (14)$$

where V_1 is the stator phase voltage in rms. The individual components of the stator voltage space vector in the excitation reference frame take the value

$$v_{d1}^e = 0 \qquad v_{q1}^e = \omega_1\Psi_1^e = \sqrt{2}V_1 = const \quad (15)$$

Eqns. 14 and 15 demonstrate that the magnitude of the stator flux is set by the stator voltage and that the stator voltage vector is $\pi/2$ in advance of the stator flux vector.

A simple way to obtain μ is therefore by measuring the stator voltage vector angle α_1 in the stationary reference frame a and subsequently subtracting $\pi/2$. The angle α_1 can be obtained by a 3-to-2 transformation of the individual stator phase voltages, yielding the stator voltage vector in the stationary reference frame and a cartesian-to-polar transformation. As is the case for the second method, for this simple technique it is necessary to measure the stator voltage. There are no machine parameters involved and the rotor position is not necessary in acquiring the field angle. However, this method is only possible with a stiff voltage source, free of fluctuations and voltage disturbances. This method is employed in the following control investigations.

3.1.3 Stator to rotor relationships: Rearranging eqn. 6 and splitting it into d-q-components together with the constraints of eqn. 3 the rotor-current components show the following interaction with the stator-current components

$$i_{d1}^e = \frac{1}{L_1}\Psi_1^e - \frac{L_m}{L_1} i_{d2}^e \tag{16}$$

$$i_{q1}^e = -\frac{L_m}{L_1} i_{q2}^e \tag{17}$$

When constant inductance values are assumed the d-component of the rotor current directly manipulates the stator-current d-component and the rotor-current q-component is a measure for the stator-current q-component. The stator flux in eqn. 16 is determined by eqn. 14.

Stator active and reactive power are calculated in terms of space vectors by the stator voltage and current in a general reference frame g as

$$P_1 = \frac{3}{2}\left(v_{d1}^g i_{d1}^g + v_{q1}^g i_{q1}^g\right)$$

$$Q_1 = \frac{3}{2}\left(v_{q1}^g i_{d1}^g - v_{d1}^g i_{q1}^g\right)$$

Applying the constraints of eqn. 15 and substituting the stator current components of eqns. 16 and 17, the stator active and reactive power in the e-frame can then be expressed as

$$P_1 = -\frac{3}{2}\frac{\sqrt{2}V_1 L_m}{L_1} i_{q2}^e \tag{18}$$

$$Q_1 = \frac{3}{2}\frac{\sqrt{2}V_1}{L_1}\Psi_1^e - \frac{3}{2}\frac{\sqrt{2}V_1 L_m}{L_1} i_{d2}^e \tag{19}$$

It can be seen that the stator active power is directly proportional to the q-component of the rotor current in the excitation reference frame and the stator reactive power is proportional to the d-component of the rotor current.

3.2 Control with position encoder

3.2.1 Transformation angle ε determination: Controlling the rotor current components in the excitation reference frame e requires the transformation of the rotor current from the rotor reference frame b into the e-frame and back. With the simple flux angle determination method as described under Section 3.1 and having the rotor position available, the transformation angle ε can be constructed as shown in Fig. 3. Subtracting $\pi/2$ from the stator voltage angle α_1 yields the stator flux angle μ, of which Θ_r is subtracted to gain the angle ε. The rotor position angle Θ_r is measured with an incremental encoder.

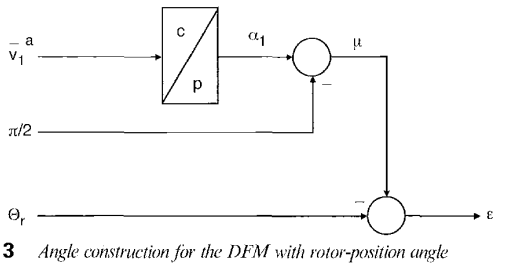

Fig. 3 *Angle construction for the DFM with rotor-position angle*

3.2.2 Inner current-control loop: The use of a voltage source inverter as the actuator unit requires the implementation of a fast current-control loop on the rotor. This current-control loop ensures that the current values, demanded by the outer control loops (power or speed), actually appear on the rotor of the DFM. The effect of the current-control loop is analysed in the following:

Resolving eqn. 6 after the stator current and substituting it in eqn. 7 delivers the rotor flux in the form of

$$\overline{\Psi}_2^e = \left(L_2 - \frac{L_m^2}{L_1}\right)\overline{i}_2^e + \frac{L_m}{L_1}\overline{\Psi}_1^e \tag{20}$$

Replacing eqn. 20 in eqn. 5 gives, for the rotor voltage in the e-frame,

$$\overline{v}_2^e = R_2\overline{i}_2^e + \left(L_2 - \frac{L_m^2}{L_1}\right)\frac{d\overline{i}_2^e}{dt} + \frac{L_m}{L_1}\frac{d\overline{\Psi}_1^e}{dt} + \mathrm{j}\omega_2\left(L_2 - \frac{L_m^2}{L_1}\right)\overline{i}_2^e + \mathrm{j}\omega_2\frac{L_m}{L_1}\overline{\Psi}_1^e \tag{21}$$

where $\omega_2 = \omega_1 - \omega_r$ is the slip frequency.

Splitting eqn. 21 into d-q and considering only the steady state ($d/dt = 0$) with ${\Psi_{q1}}^e = 0$ leads to

$${v_{d2}^e}^* = R_2 i_{d2}^e - \omega_2\left(L_2 - \frac{L_m^2}{L_1}\right) i_{q2}^e \tag{22}$$

$${v_{q2}^e}^* = R_2 i_{q2}^e + \omega_2\left(L_2 - \frac{L_m^2}{L_1}\right) i_{d2}^e + \omega_2\frac{L_m}{L_1}\Psi_1^e \tag{23}$$

The components v_{d2}^{e*} and v_{q2}^{e*} are the rotor voltage components in the e- frame which are necessary to ensure the desired rotor current values i_{d2}^e and i_{q2}^e in the rotor circuit. As can be seen, the second terms in these equations constitute cross coupling terms and the third term in eqn. 23 is equivalent to a speed-dependent induced e.m.f. term associated with the stator flux. The cross coupling terms in eqns. 22 and 23 are an order of magnitude smaller than the back e.m.f term. Their minor influence upon the control is catered for by the PI-controller in each axis. However, the third term in eqn. 23 acts as a disturbance to the output of the PI-controller in the q-axis. It is possible to compensate for the influence of the back e.m.f. term by choosing high PI-controller gains but a steady-state tracking error will persist [13]. The tracking error can be eliminated by adding a feed-forward term to the output of the q-axis controller with the value of

$$feed\ forward = \omega_2\frac{L_m}{L_1}\Psi_1^e \tag{24}$$

This also results in easier tuning. The complete current-control structure of the DFM with a position encoder is shown in Fig. 4.

Experimental results for the inner current-control loop of the DFM are presented in Figs. 5 and 6. Fig. 5 shows results for a step change in the d-component of the rotor

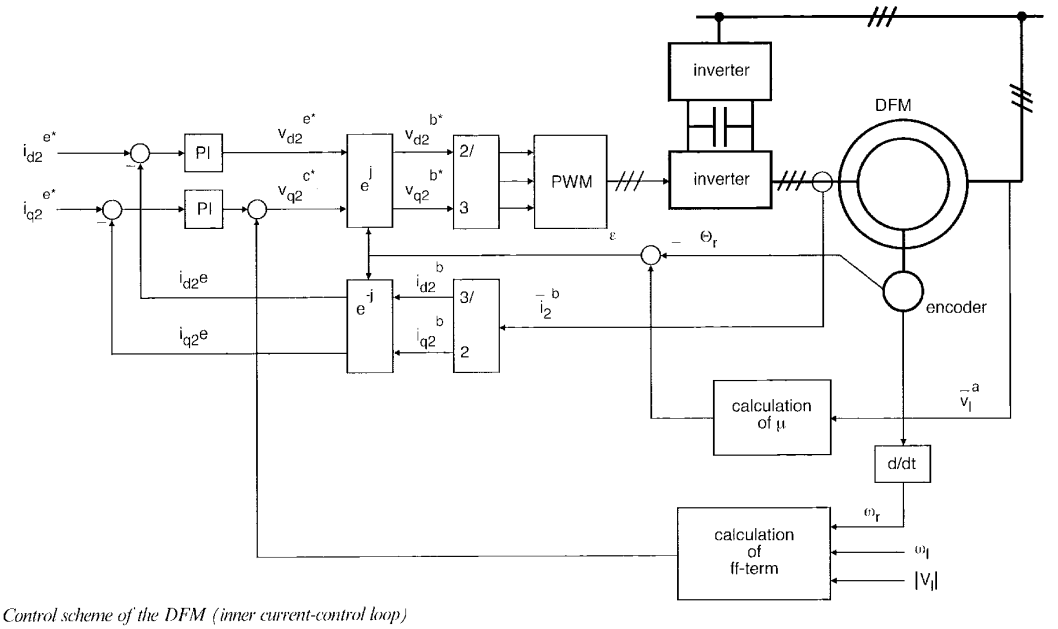

Fig. 4 *Control scheme of the DFM (inner current-control loop)*

current. The demand value for the d-axis rotor current in the e-frame was set to perform a sudden step from 0A to 4A and back to 0A, while the q-axis current demand was left at a constant value of 2A. Measured quantities are the rotor current components in the e-frame (denoted as 'i_{d2}^{e}' and 'i_{q2}^{e}') and the stator active P_1 and reactive power Q_1. It can clearly be seen that, due to that step change, the stator reactive power is controlled. The slight variation in the stator active power during the step change is the effect of the neglected stator resistance. Although the effect of the stator resistance can be seen, it is still small enough to justify the neglect of it. Negative active power means generating mode, i.e. power flows from the DFM towards the grid. Positive stator reactive power indicates a lagging stator power factor, so that inductive power flows from the grid towards the DFM as excitation power, whereas a negative Q_1 indicates leading stator power factor. In this case the excitation power for the DFM is supplied via the rotor.

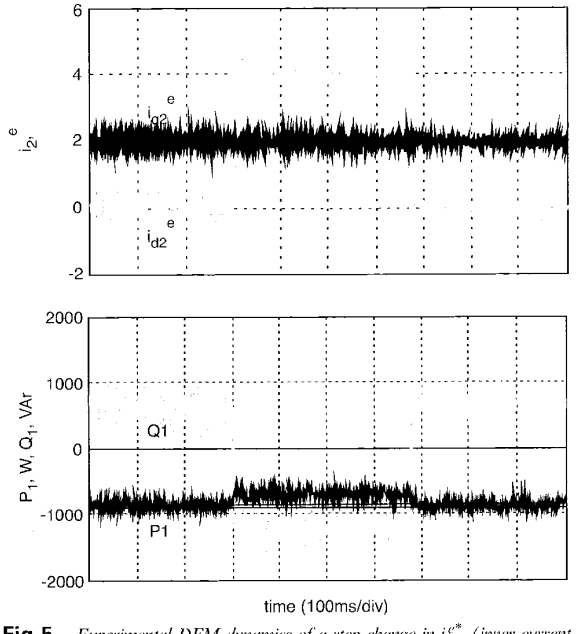

Fig. 5 *Experimental DFM dynamics of a step change in i_{d2}^{e*} (inner current-control loop)*
Step in i_{d2}^{e*} = 0 to 4 to 0A; i_{q2}^{e*} = 2A; n_m = 1140r/min

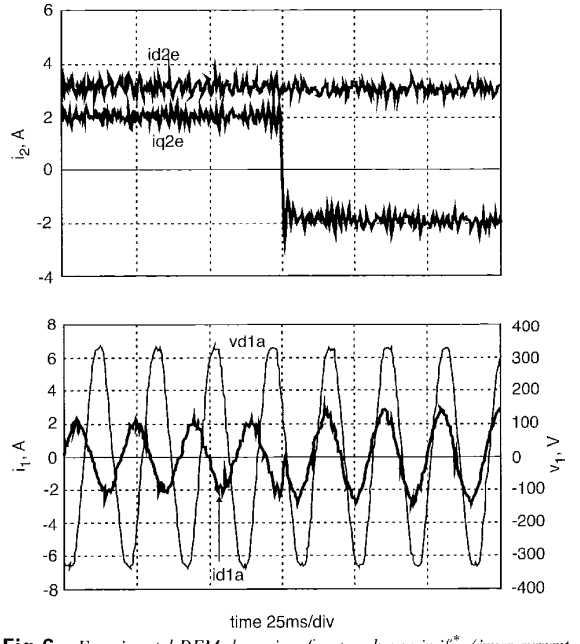

Fig. 6 *Experimental DFM dynamics of a step change in i_{q2}^{e*} (inner current-control loop)*
Step in i_{q2}^{e*} = 2 to 2A; i_{d2}^{e*} = 3A; n_m = 1450r/min

Fig. 6 shows a step response of the q-axis rotor current component together with the stator voltage ('v_{d1}^{a}') and stator current ('i_{d1}^{a}') of the same stator phase winding, in the stator reference frame a. The phase change between stator voltage and current with the change in magnitude of the stator current clearly displays the fundamental principle of field orientation which is a sudden step change from one steady-state condition into another [14].

3.2.3 Outer power control loop: The proportionality of the rotor current components to the stator active and

reactive power allows the inner current-control loop to be supplemented with an outer power control loop in a cascaded manner. The output of the PI-controller for stator active power is fed as a demand value for the q-axis rotor current component of the inner current-control loop. The output of the reactive power controller serves as an input to the d-axis current controller. Actual values of the stator active and reactive power are calculated from the measured stator voltage and current in the stationary reference frame a.

Fig. 7 illustrates experimental results for step changes in the active demand, with no recognisable influence in the reactive power, and Fig. 8 shows the results for a step in the reactive power demand with a similar decoupled control performance.

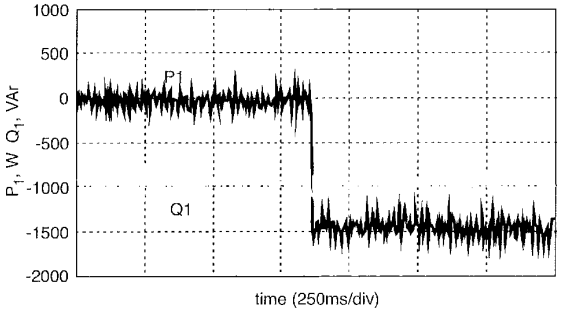

Fig. 7 *Experimental DFM dynamics of a step change in P_1^* (outer power-control loop)*
Step in P_1^* = 0 to −1.5kW; Q_1^* = −1kVAr; n_m = 1650r/min

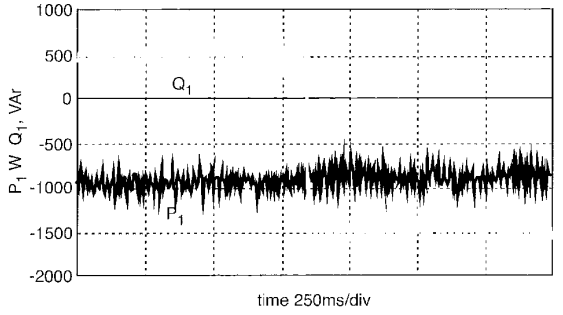

Fig. 8 *Experimental DFM dynamics of a step change in Q_1^* (outer power-control loop)*
Step in Q_1^* = 0.5 to −1.5kVAr; P_1^* = −1kW; n_m = 1200r/min

3.2.4 Outer speed control loop: The implementation of an outer power control loop is mainly employed in the generating mode of the DFM, but for other applications, such as pump drives, torque or speed control may be appropriate. Based on eqn. 2 it is shown that, in the field-oriented reference frame, the torque is proportional to the q-axis rotor current. An outer speed or torque controller, depending on the application, delivers the demand value for the q-axis rotor component. With this type of application, the input to the d-axis current controller is mostly set to a fixed value to give a certain stator reactive power value.

Fig. 9 illustrates experimental measurements for a speed-control application. A demand speed ramp from 1000 to 1650r/min and back is carried out at no-load. The rotor current d-component is set to 3A. As eqn. 2 suggests, the torque is manipulated by the q-component in order to follow the demanded speed value, whereas the d-component is held constant across the speed variation.

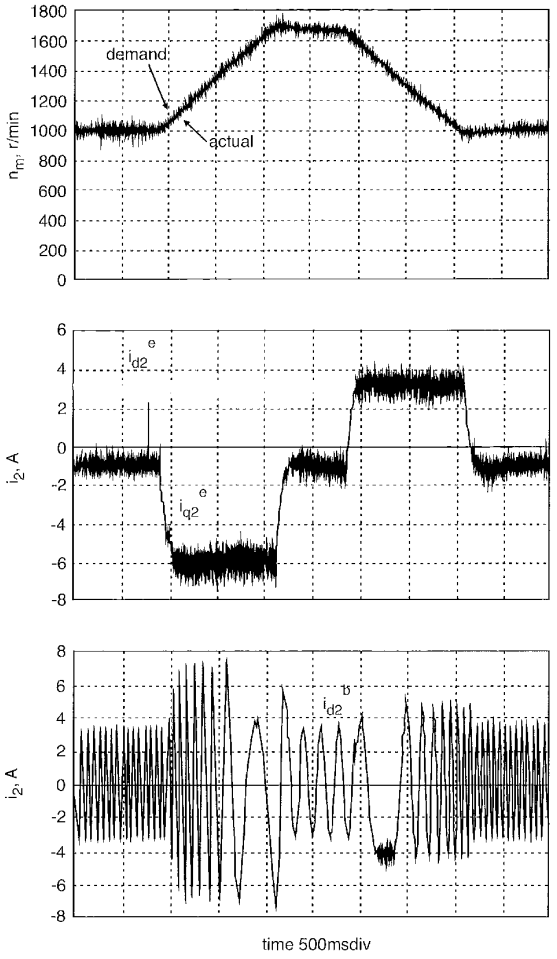

Fig. 9 *Experimental DFM dynamics (outer speed-control loop at no-load)*
i_{q2}^{e*} = 3A; n_m = 1000–1650r/min

3.3 Control without encoder

This Section covers the control of the DFM without a positions sensor. The sensorless scheme is initially based on the method as introduced in [9], which has limitations for low rotor current magnitudes and can only be utilised for power control. As a further step, the sensorless method is extended to be applicable as a sensorless speed-control scheme. Alternatively, a different method on how to construct the transformation angle ε is introduced.

3.3.1 Transformation angle e determination — method A: Without having the rotor position angle Θ_r available there has to be a different solution found for constructing the transformation angle ε. As demonstrated in [9] this can be done with the help of the proportionality between the stator and the rotor current. Regarding eqns. 16 and 17, the rotor current components in the e-frame can be calculated from the stator current components as

$$i_{d2calc}^e = \frac{1}{L_m}\Psi_{d1}^e - \frac{L_1}{L_m} i_{d1}^e \tag{25}$$

$$i_{q2calc}^e = -\frac{L_1}{L_m} i_{q1}^e \tag{26}$$

The stator flux value follows from eqn. 14 with V_1 and ω_1 as constants. With this method, the stator current components have first to be rotated from the stationary a-frame

into the excitation frame e. This is possible since the stator flux angle μ is known from the measurement of the stator voltage, as Fig. 3 shows. A cartesian-to-polar transformation of the calculated rotor current in the e-frame allows the angle χ to be derived, which is included in Fig. 2. The measurement of the rotor current in its natural reference frame b enables the angle β_2 to be calculated. With the knowledge of the angles χ and β_2 the transformation angle ε can be calculated as $\varepsilon = \beta_2 - \chi$. This angle construction method (referred to as method-A) is illustrated in Fig. 10.

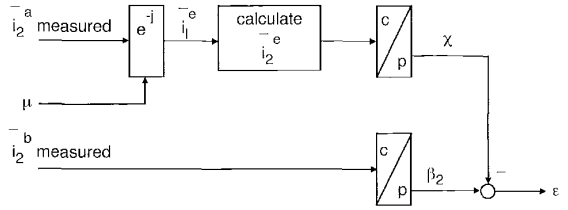

Fig. 10 *Angle construction of the sensorless DFM from current measurements (method A)*

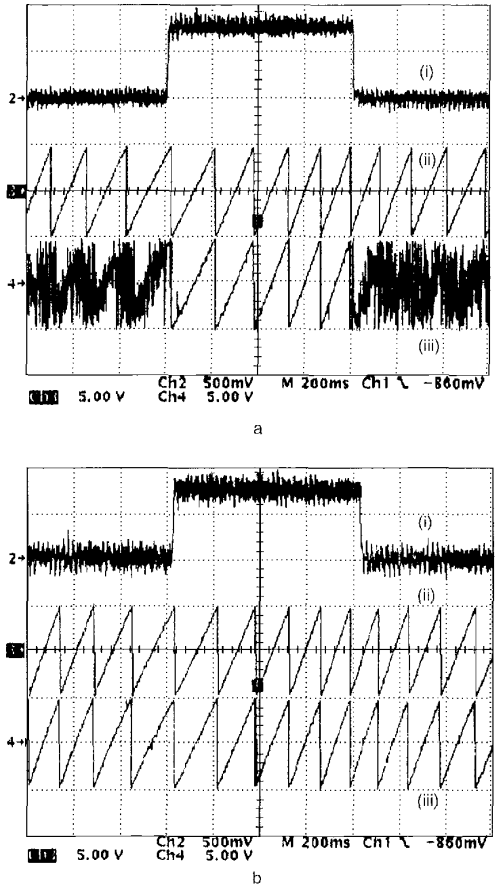

Fig. 11 *Experimental, actual and estimated angle ε with a step in i_{q2}^e from 0A to 2A and back to 0A*
a i_{d2}^e = 0A
b i_{d2}^e = 3A
(i) i_{q2}^e (1.33A/div)
(ii) ε actual (3.22rad/div)
(iii) ε extimated (3.22rad/div)

Fig. 11 displays two plots of the inner current-control loop for two different settings of the rotor-current demand values. In both cases the rotor-current q-component performs a step from 0A to 2A and back to 0A, but the d-component is initially set to 0A and then to 3A in Fig. 13*b*. A comparison between the actual and the calculated or estimated angle ε shows that, during the time when i_{d2}^e and i_{q2}^e are 0A, the angle ε cannot be estimated properly. This is because the ripple in the measured rotor-current components does not allow a correct determination of the angle β_2 in this case. It is different when i_{q2}^e is at 2A, then the angle β_2 and ε can be calculated. As a consequence, it has to be ensured that the rotor current magnitude $|i_2^b|$ is always large enough to identify the angle β_2 properly. As Fig. 13*b* shows with i_{d2}^e at 3A, there are no difficulties anymore during the time when i_{q2}^e is at 0A. The angle ε can always be estimated, and the actual and estimated angles indicate good agreement. The best way to achieve a 'safe' angle estimation is probably by setting i_{d2}^e to a certain minimum current level and leaving i_{q2}^e free for control purposes. In that way it is not possible to control the stator reactive power any more, since it is set to a constant level, but it is ensured that the rotor-current magnitude is always large enough.

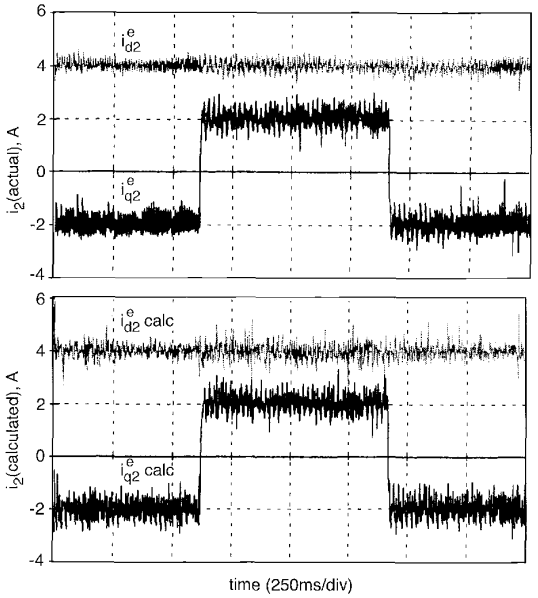

Fig. 12 *Sensorless experimental DFM dynamics (inner current-control loop)*
i_{d2}^{e*} = 4A; i_{q2}^{e*} = -2 to 2 to 2A

Sensorless inner current-control loop: Fig. 12 shows experimental results for the sensorless current-control loop. The d-component demand of the rotor current in the e-frame is set to 4A to ensure the estimation of the rotor angle for all possible q-component values. The demand for the q-axis component performs a step change from –2A to 2A and back to 2A. It is illustrated that the calculated rotor current components i_{d2calc}^e and i_{q2calc}^e coincide well with the actual measured rotor current components. However, the ripple content on the calculated rotor currents is slightly higher than on the actual ones. Fig. 13 gives the sensorless control scheme for the DFM.

Sensorless outer power-control loop: To extend the inner current-control loop to an outer power-control loop, a PI-controller for the stator active power is cascaded onto the q-axis of the inner current-control loop to deliver the demand q-axis rotor current. Again, i_{d2}^{e*} is kept at 4A to ensure a proper angle estimation. Experimental results in Fig. 14 display that, with the sensorless arrangement, the ripple in the stator active power and the associated q-component of the rotor current exhibit a significant ripple content. This ripple does not appear in the d-axis of the control loop, since there is no outer feedback for it. Despite the

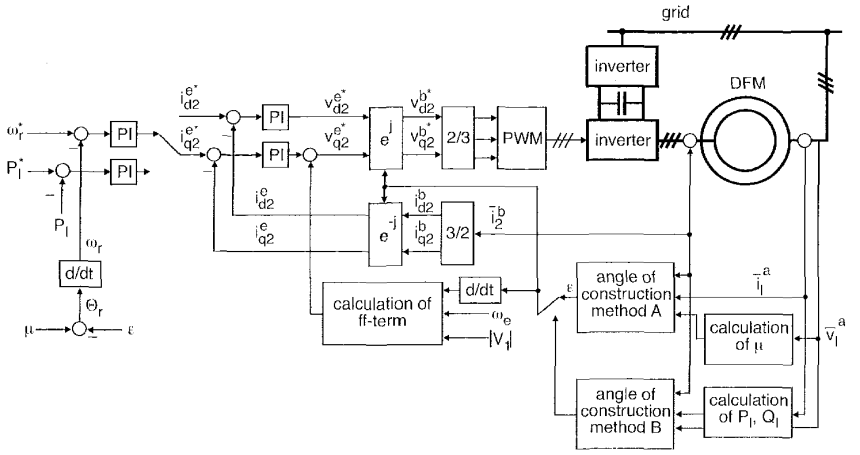

Fig. 13 *Sensorless DFM control structure (method A and method B)*

increased ripple, sensorless power control can be performed.

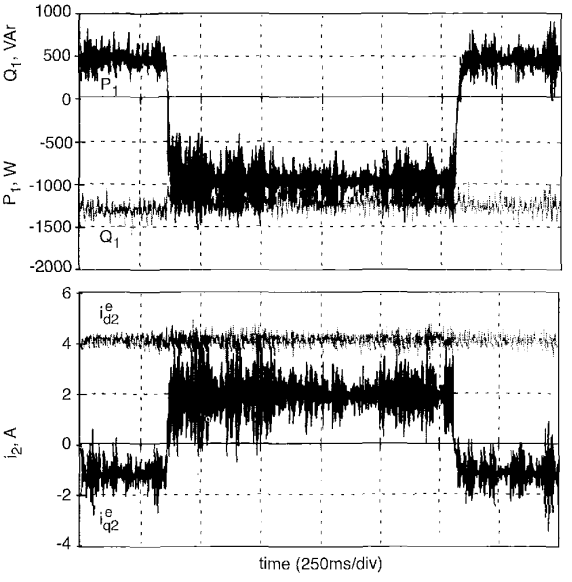

Fig. 14 *Sensorless experimental DFM dynamics for P_l-control (method A)*
$i_{d2}^{e*} = 4$A; $P_l^* = 500$ to 1000 to 500W

Sensorless outer speed-control loop: Sensorless control in this paper and [9] has so far only dealt with the application of the control for a power-control loop. However, by further developing the applied principle a way for a sensorless speed-control loop can be derived.

Considering the angles in Fig. 2, it can be seen that the rotor position angle Θ_r can be estimated from $\Theta_r = \mu - \varepsilon$. The angle μ is known from the stator-voltage measurement and the angle ε can be constructed as displayed in Fig. 10. Differentiating the acquired rotor-position angle delivers the rotor speed in electrical rad/s as

$$\omega_r = \frac{d\Theta_r}{dt}$$

This signal can be used to form a speed feed-back and thus to apply a sensorless speed control to the DFMI.

Fig. 15 shows the actual measured and the estimated rotor position angle, Θ_r. Both angles are in very close agreement. However, the estimated Θ_r displays a more coarse waveform compared to the actual signal.

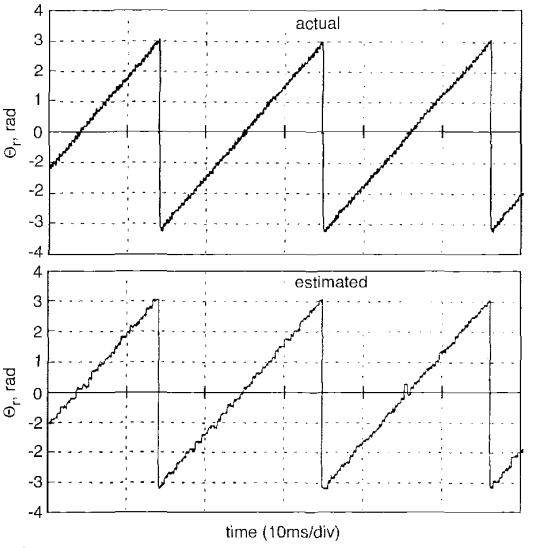

Fig. 15 *Actual and estimated rotor position angle Θ_r*

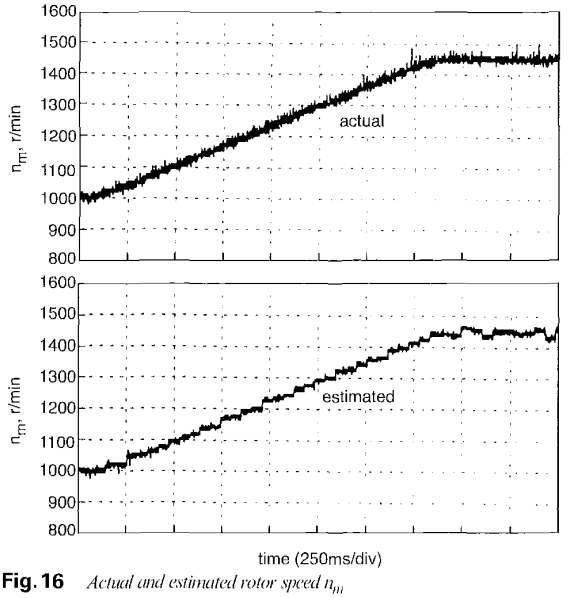

Fig. 16 *Actual and estimated rotor speed n_m*

The actual and the estimated speed signal for a speed ramp from 1000 to 1460r/min is displayed in Fig. 16. Here,

the estimated speed signal shows a 'stepwise' speed variation compared to the actual signal, owing to the following reason: the differentiation of the estimated rotor-position angle for every switching cycle yields a very spiky speed signal with the mean value of the actual speed. That is because the gradient of the estimated rotor position angle is not monotonic, as is the case with the actual rotor-position angle obtained from the encoder signals. In other words, the successive rotor position values for every cycle may not increase in a steady manner. The time for differentiation is therefore increased to 18 cycle times to reduce this problem. The calculated speed signal therefore remains constant for 18 cycle times and allows only a stepwise variation.

The averaging 18 cycle times are also applied for differentiation of the estimated angle ε to calculate the slip frequency for the feed-forward component in the q-axis.

Sensorless speed control results are shown in Fig. 17. The speed demand performs a speed ramp from 1000 to 1650r/min and back, covering sub- and supersynchronous speed. The estimated speed signal, derived from the calculated rotor position angle Θ_r, in Fig. 17 is used as a feedback for the PI-controller in the q-axis. It can be seen that the q-axis current i^e_{q2} contains 'spike-blocks' over the 18 cycle times used for the speed calculation. The d-axis current remains unaffected. Despite the stepwise speed values, the DFM follows the desired speed ramp surprisingly well. Compared to the speed-loop results of the DFM with a sensor, in Fig. 9, the dynamic speed variation had to be reduced for the sensorless case to cater for the averaging 18 cycle calculation.

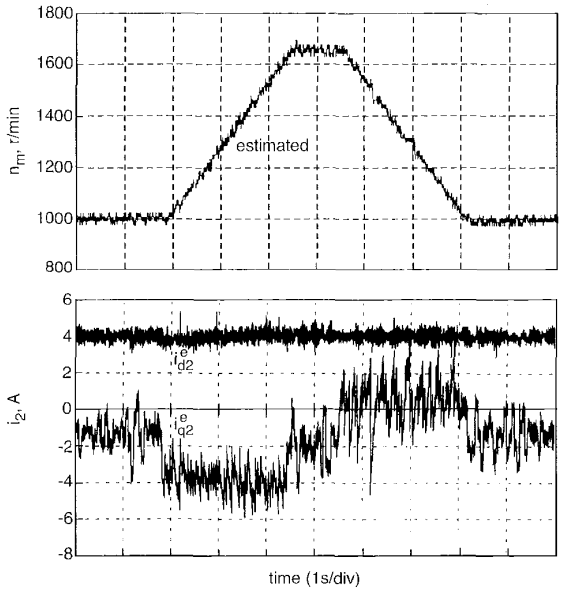

Fig. 17 *Sensorless experimental DFM dynamics for speed control (method A)*
i^e_{d2} = 4A; n_m = 1000 to 1650r/min; no-load

3.3.2 Transformation angle e determination — method B: The method so far ('method A') uses the stator currents for the calculation of the rotor current and hence the angle χ. Analysis in Section 3.1 has shown that the rotor current components are proportional to the stator active and reactive power. Consequently, instead of the stator current, the stator active and reactive power could be used to calculate the rotor current in the form

$$i^e_{d2calc} = \frac{1}{L_m}\Psi^e_{d1} - \frac{2}{3}\frac{L_1}{\sqrt{2}V_1 L_m}Q_1 \qquad (27)$$

$$i^e_{q2calc} = -\frac{2}{3}\frac{L_1}{\sqrt{2}V_1 L_m}P_1 \qquad (28)$$

The resulting angle construction method ('method B') is illustrated in Fig. 18. In comparison to method A, the angle construction method in Fig. 10 does not contain the transformation block necessary for the stator current. Experimental results with this method lead to similar results as obtained with method A.

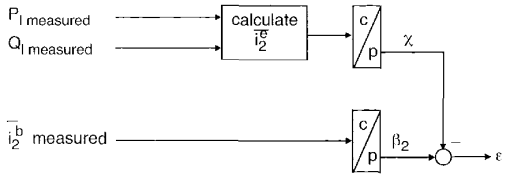

Fig. 18 *Angle construction method of the sensorless DFM from power measurements (method B)*

4 Conclusions and recommendations

This paper describes stator flux oriented control structures for a DFM, with and without position encoder. It is shown that a sensorless control arrangement is feasible not only for power-control application but for speed-control applications of the DFM.

The sensorless power-control scheme implies that the d-axis current component is set to a minimum constant value to ensure a safe transformation angle determination, as shown in this paper. This clearly limits the manipulation of the stator reactive power. Another control block within the power-control loop may overcome this problem. This control block could allow the variation of the d-axis current component as long as the magnitude of the rotor current, composed of d-q-axis current components, stays above a minimum value. This may be investigated in further work on the sensorless control of the DFM.

Additional work should also focus on the performance improvement of the sensorless control arrangement. One way could be by employing a different method of filtering, such as moving average, first or second-order filters, of the estimated rotor-position angle. An increased angle resolution may also improve the speed signal. The implemented code has an angle resolution of 0.9° defining 400 values for the angle range 0–2π.

Further work may moreover address a performance evaluation of the sensorless control scheme in the wind-power application, with its specific idiosyncrasies such as blade characteristics, wind gusts and tower shadow.

5 Acknowledgments

The authors wish to thank Microtech Ltd., Gateshead, and Robert Bosch GmbH, Erbach, for support and hardware donation. B. Hopfensperger wishes to thank the Department of Electrical and Electronic Engineering and the University of Newcastle for financial support.

6 References

1 WALLACE, A.K., SPEE, R., and LAUW, H.K.: 'The potential of brushless doubly-fed machines for adjustable speed drives'. Proceedings of the IEEE Annual Pulp and Paper Industry technical conference, 1990, pp. 45–50

2 MAYER, C.B.: 'High response control of stator watts and vars for large wound rotor induction motor adjustable speed drives', *IEEE Trans. Ind. Appl.*, 1983, **19**, (5), pp. 736–743

3 LEONHARD, W.: 'Field oriented control of a variable speed alternator connected to the constant frequency line'. Proceedings of the IEEE conference on *Control of power systems*, 1979, pp. 149–153

4 MASMOUDI, A., TOUMI, A., KAMOUN, M.B.A., and POLOUJADOFF, M.: 'On the stator-flux-oriented control of a doubly-fed synchronous machine', *Eur. Trans. Electr. Power Eng.*, 1995, **5**, (1), pp. 23–31
5 HELLER, M., and SCHUMACHER, W.: 'Stability analysis of doubly-fed induction machines in stator flux reference frame'. Proceedings of EPE'97, 1997, pp. 2.707–2.710
6 PENA, R., CLARE, J.C., and ASHER, G.M.: 'Doubly-fed induction generator using back-to-back PWM converters and its application to variable-speed wind-energy generation', *IEE Proc., Electr. Power Appl.*, 1996, **143**, (3), pp. 231–241
7 ATKINSON, D.J., LAKIN, R.A., and JONES, R.: 'A vector controlled doubly-fed induction generator for a variable-speed wind turbine application', *Trans. Inst. Meas. Control*, 1997, **19**, (1), pp. 2–12
8 EDVARDSEN, P.A., NESTLI, T.F., and KOLSTAD, H.: 'Steady state power flow and efficiency optimising analysis of a variable speed constant frequency generating system'. Proceedings of EPE'97, 1997, pp. 2.691–2.694
9 ARSUDIS, D., and VOLLSTEDT, W.: 'Sensorlose Regelung einer doppeltgespeisten Asynchronmaschine mit geringen Netzrückwirkungen', *Arch. Elektrotech.*, 1990, **74**, pp. 59–97
10 XU, L., and CHENG, W.: 'Torque and reactive power control of a doubly-fed induction machine by position sensorless scheme', *IEEE Trans. Ind. Appl.*, 1995, **31**, (3), pp. 636–642
11 MOREL, L., GODFROID, H., MIRZAIAN, A., and KAUFFMANN, J.M.: 'Double-fed induction machine: converter optimisation and field oriented control without position sensor', *IEE Proc., Electr. Power Appl.*, 1998, **145**, (4), pp. 360–368
12 LEONHARD, W.: 'Control of electric drives' (Springer Verlag, Berlin, 1996, 2nd edn.)
13 HOLTZ, J.: 'Pulsewidth modulation for electronic power conversion', *Proc. IEEE*, 1994, **82**, (5), pp. 1194–1214
14 HUGHES, A., CORDA, J., and ANDRADE, D.A.: 'Vector control of cage induction motors: a physical insight', *IEE Proc., Electr. Power Appl.*, 1996, **143**, pp. 59–68